Techniques for Intense-Proton-Beam Profile Measurements*

J. D. Gilpatrick

Los Alamos National Laboratory
Los Alamos, NM 87545

Abstract. In a collaborative effort with industry and several national laboratories, the Accelerator Production of Tritium (APT) facility and the Spallation Neutron Source (SNS) linac are presently being designed and developed at Los Alamos National Laboratory (LANL). The APT facility is planned to accelerate a 100 mA H^+ cw beam to 1.7 GeV and the SNS linac is planned to accelerate a 1 to 4 mA-average, H^-, pulsed-beam to 1 GeV. With typical rms beam widths of 1 to 3 mm throughout much of these accelerators, the maximum average-power densities of these beams are expected to be approximately 30 and 1 MW-per-square millimeter, respectively. Such power densities are too large to use standard interceptive techniques typically used for acquisition of beam profile information. This paper will summarize the specific requirements for the beam profile measurements to be used in the APT, SNS, and the Low-Energy Development Accelerator (LEDA) — a facility to verify the operation of the first 20 MeV section of APT. This paper will also discuss the variety of profile measurement choices discussed at a recent high-average-current beam profile workshop held in Santa Fe, NM, and will present the present state of the design for the beam profile measurements planned for APT, SNS, and LEDA.

HIGH AVERAGE-BEAM-CURRENT ACCELERATORS

In partnership with industry and several other national laboratories, LANL is designing two high-average-current accelerators. The APT linac, which will be built at the Savannah River Site Laboratory, will accelerate a 100 mA cw H^+ beam to 1.7 GeV. The SNS linac, which will operate at the Oak Ridge National Laboratory, will accelerate a 1 to 4 mA-average H^- pulsed beam to 1 GeV.

The schematic representation in Figure 1 shows the APT accelerator general layout (1). During the first 211 MeV, beam is accelerated with room-temperature accelerating structures followed by a series of short superconducting accelerating structures (2). The

* Work supported by the U.S. Department of Energy.

DC beam is initially extracted from the source at 75 keV. It is then bunched at 350 MHz and accelerated to 6.7 MeV with an 8 m-long radio frequency quadrupole (RFQ). A series of differently configured coupled-cavity drift-tube linacs (CCDTLs) and coupled-cavity linacs (CCLs) increase the beam's energy to approximately 100 MeV and 211 MeV, respectively. Up to an energy of 469 MeV, the superconducting linac (SCL) is composed of a series of cryogenic modules each of which is composed of either β=0.64 superconducting multi-cell cavity accelerators. Above 469 MeV, β=0.84 multi-cell-cavity accelerators are used. The beam is then transported by a high-energy beam transport (HEBT) to either a tune-up 2% duty-factor beam stop or the target/blanket assembly where the tritium is produced.

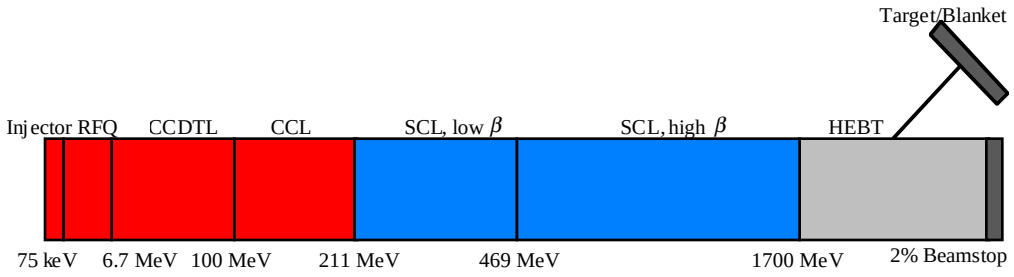

FIGURE 1. The APT accelerator is composed if a series of normal conducting(room temperature) and superconducting accelerator structures. After acceleration to 1700 MeV the cw beam is transported to the target/blanket facility where the tritium is produced.

At Los Alamos, we will be installing and commissioning the first 20 MeV (Fig. 2) of the APT accelerator in a facility called the LEDA (3). This facility is presently being assembled to perform the first experiments that verify the operation of the RFQ. The RFQ verification process will take place during three experiments: the first experiment will provide an initial indication of the RFQ by sustaining 8 hours of operation of a 100 mA cw beam, the second experiment will operate the RFQ for an extended period of time, and a third experiment will test the transverse-matching capability of the CCDTL lattice to the RFQ output beam. Later experiments will verify operation of the CCDTL.

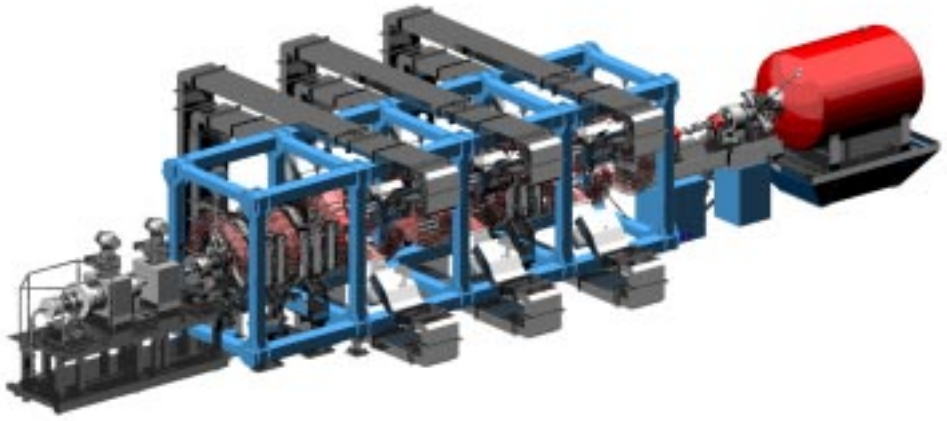

FIGURE 2. The first LEDA experiment configuration that includes the 75 keV injector,the 6.7 MeV RFQ, a short HEBT, and a 670 kW beamstop, is shown.

The SNS accelerator-facility concept is sketched in Figure 3. It consists of a 65 keV H^- injector, a 2.5 MeV RFQ, and a short medium-energy beam transport (MEBT) which matches the beam to a DTL that accelerates the beam to 20 MeV. The beam is then accelerated to 1 GeV by a CCDTL and CCL (4).

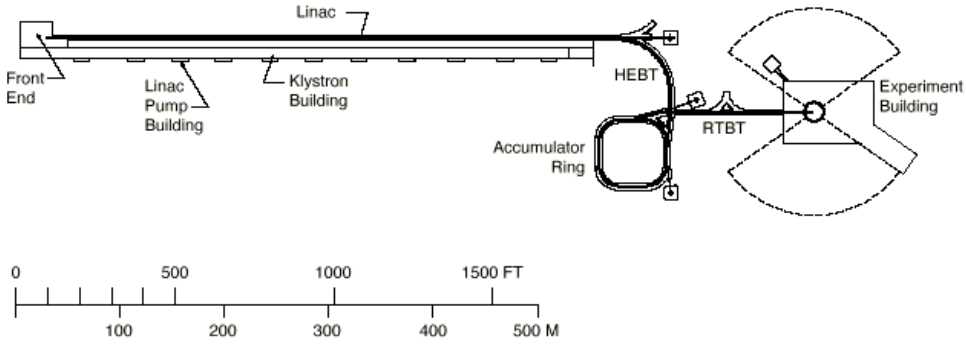

FIGURE 3. The SNS facility contains a room temperature linac consisting of an RFQ, DTL, CCDTL, and CCL. The 1 GeV beam is then transported to a ring where it is accumulated to a <1 μs pulse and transported to a neutron-production target. The short pulse of neutrons are used for diverse research applications.

Table 1 summarizes the beam commissioning and operational parameters of both facilities. While the APT cw average current is 25 to 100 times greater than the SNS average beam current, due to the SNS duty factor, its peak and average macropulse current is 1/4 and 1/7, respectively, of APT. Also note that the rms beam widths are similar for both facilities, and therefore, both facilities have very high beam-current densities.

TABLE 1. Summary of the APT and SNS Operational Beam Parameters

Beam Parameter	APT	SNS
Particle	H^+	H^-
Maximum average current (mA)	100	1, 2, 4
Maximum average macropulse current (mA)	100	18
Macropulse beam repetition rate (Hz)	cw, 1–10	60, or less
Macropulse length (ms)	cw, 1.0–0.1	1.04, or less
Chopped beam period (ns)	NA	841
Chopper transmission (%)	NA	65
Bunching frequency (MHz)	350	402.5, 805
Source energy (keV)	75	65
Output energy (GeV)	1.7	1.0
Transverse rms emittance, norm. (π mm-mrad)	0.16–0.19	0.14–0.17
Typical transverse rms widths (mm)	0.8 to 2.1	0.9 to 1.7

BEAM PROFILE MEASUREMENT MOTIVATION

The motivation for measuring beam profiles throughout these accelerators is primarily due to the requirement for minimizing beam loss in the accelerator. Lost beam will result in unacceptable radioactivation of the accelerator and beam line structures. For APT, reducing beam losses throughout the accelerator to ~0.1 nA/m or 0.1 mA total losses is an operational goal. Lost beam can be a result of a mismatch between the beam's Twiss parameters or betatron funtions and the accelerator's acceptance. Such a mismatch can cause the beam envelope to "flutter" (oscillate unevenly), producing beam transverse-distribution extent or "halo" growth and, in some cases, rms-width growth. Additional mismatch errors and magnet-fringe-field errors can further spread beam halo and increase beam losses. Figure 4 shows a typical representation of how these mismatches can cause a halo growth (5). The figure on the left shows a properly matched beam to a periodic transverse lattice. The figure on the right shows the result of a 50% mismatch; a halo has formed outside the beam core.

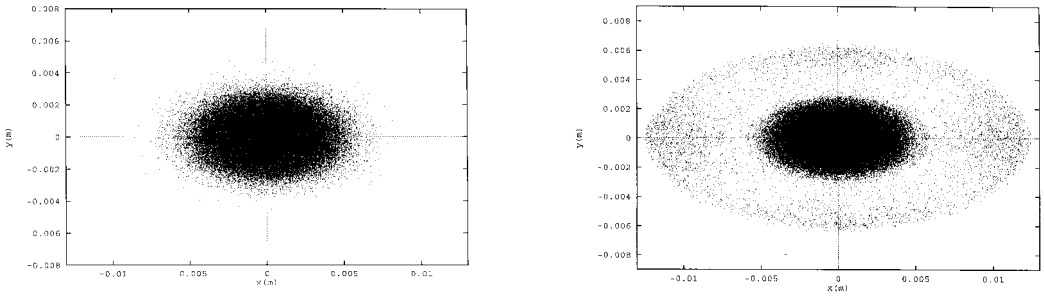

FIGURE 4. This figure shows a typical representation of the extent to which mismatches can cause halo growth. The figure on the right shows the transverse profile of a beam well-matched to a transverse periodic lattice. The figure on the right shows that a 50% mismatch can cause halo growth.

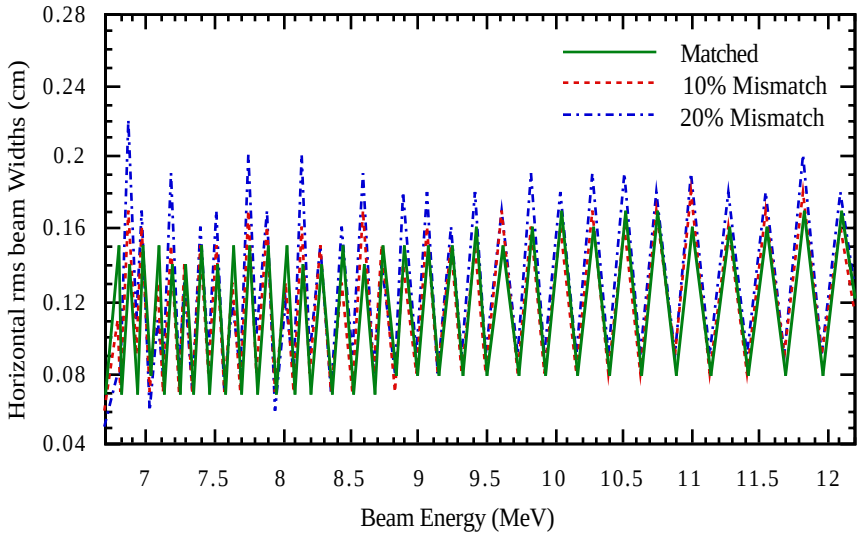

FIGURE 5. This graph shows the horizontal rms beam width as a function of beam energy in the CCDTL (or as a function of location in the CCDTL lattice). The three conditions plotted are a properly matched RFQ output beam, a 10% mismatched RFQ output beam, and a 20% mismatched RFQ output beam.

Another view of the mismatched beam condition can be seen in Figure 5. In this graph, the rms beam width is plotted versus beam energy within the APT CCDTL after the RFQ for three conditions: a matched beam, a 10% mismatched beam located at the RFQ/CCDTL interface, and a 20% mismatched beam at the same interface (6). Under the matched condition, the beam envelope oscillates <0.3 mm. Under the 10%- and 20%-mismatched conditions, the beam flutters <0.4 mm and <1 mm, respectively. The difference between these three conditions becomes less apparent after the beam is transported through 10 or more focus/defocus lattice periods (shown in the graph as several MeV of energy gain). At these lower energies, if the mismatch is sufficiently large, the rms beam width also increases after 10 or more lattice periods.

There are several methods for determining if the beam is mismatched. The method selected for APT measures a series of beam profiles at transverse-lattice locations in areas of the accelerator where beam mismatches are likely to occur. These likely locations for mismatched-beam include the region between the RFQ and CCDTL, and between the CCL and SCL. Multiple profiles can either be analyzed for minimum rms flutter after a mismatch or the profile rms widths can be fit in a least-squared-error sense to the simulated beam trajectory. Furthermore, if each profile is acquired over the range of about 2.5 rms widths, some small portion of the mismatched-beam-dependent halo may be directly sampled. Finally, in some of these locations within the accelerator, specific beam-halo measurements will be performed to acquire information on the far outer edges of the beam distributions (e.g. about 3 to 5 rms widths) (7).

PROFILE MEASUREMENT REQUIREMENTS FOR APT

The requirements for the APT profile measurements are summarized in Table 2. As previously stated, the “full” APT profile measurement, as defined by ~2.5 rms widths, must be measured because these “full” distribution measurements allow for the observation of slight mismatch conditions. Of course, there are the usual beam-line-location and space limitations that restrict the locations at which the profile measurements can be made. These measurements must be sufficiently robust and reliable. For example, each type of beam line device must have at least a one-year expected lifetime with little or no preventative maintenance required.

TABLE 2. Summary of the APT Profile Measurement Requirements

Measurement Parameter	Requirement
Maximum cw beam current density (mA/cm2)	~50 to ~2000
Beam energy (MeV)	0.75 to 1700
Beam current dynamic range (mA)	<10 to 110
rms width range (mm)	0.3 to ~5
rms width precision (mm)	1 % of rms width
rms width accuracy	~5% of rms width
“Full” distribution range	~2.5 rms widths
Pixel size	1% of distribution peak by 20% of rms width
Acquisition time (s)	≤ 60, prefer ≤1

SURVEY OF PROFILE MEASUREMENT CANDIDATES

At a recent Intense Beam Profile Workshop held in Santa Fe, NM, a variety of beam profile measurement techniques were discussed and analyzed for their application to the APT and SNS accelerator beam profile measurements. The profile measurement techniques discussed at this workshop included various types of interceptive and noninterceptive techniques and are reviewed in the latter half of this paper.

Traditional Interceptive Profile Measurements

Even during low-duty-factor pulsed-beam operation, APT beams are too intense for traditional interceptive techniques such as harps, slow wire scanners, or viewscreens. Figure 6 shows a calculation for the temperature of a 0.14 mm-SiC fiber placed in the APT linac beam. This calculation was generated for a 4 Hz, 0.15 ms, 100 mA, 1700 MeV beam with typical peak current densities of 1.6 A/cm^2 and the calculation assumes that fiber cooling only takes place through thermal radiation. Peak temperatures of >1600K are seen even during these very low duty factor conditions, and furthermore, during cw-beam operation, the fiber will vaporize within a few milliseconds. Is this pulsed-beam fiber temperature too high a temperature for a SiC fiber or wire? Figure 7 shows manufacturing data of SiC fiber strength versus fiber temperature. This graph suggests that the above pulsed beam fiber temperature is, indeed, too great. These manufacturing data were acquired in 1 atmosphere of air and argon, a harsher environment than what is expected for the APT and SNS evacuated beam lines, show that the SiC fiber's strength degrades by a factor of three at temperatures of ~2000°F (1400 K). Even though one expects the fiber strength degradation to be less in the evacuated beam line environments, the conservative approach for wire scanner and harp designs is to never allow SiC fibers reach temperatures greater than ~1400 K. The simulation in Figure 6 shows the fiber will periodically reach temperatures well past this safe operating temperature during even very-low-duty factor conditions, let alone cw–beam conditions.

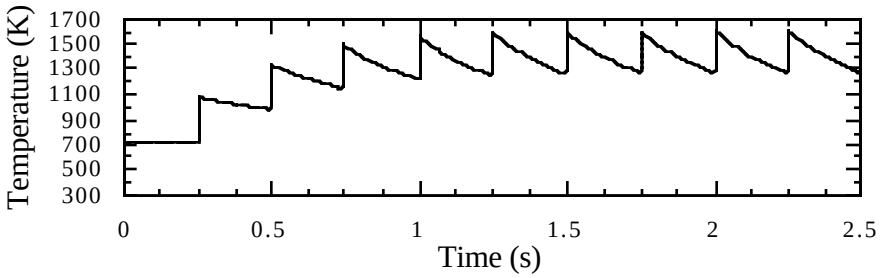

FIGURE 6. A calculation that shows the temperature of a SiC fiber placed in the APT 1.7 GeV beam. The beam is pulsed at 4 Hz with a 0.15 ms long pulse and a current density of 1.6 A/cm^2.

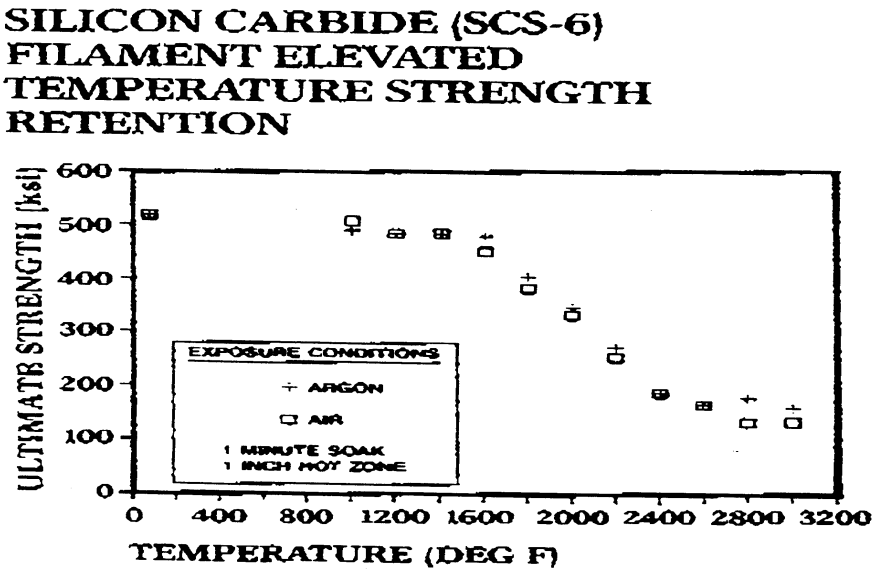

FIGURE 7. This graph depicts Textron System Division manufacturing data of 0.14 mm SiC fiber strength versus fiber temperature. These data were acquired in an environment of 1 atmosphere of air and argon (8).

Limitations of pulsed-beam operation are further reduced during the transverse lattice-tuning process in which beam widths will be smaller than nominal beam conditions. These smaller beams will increase the current densities and result in even higher peak fiber temperatures and likely fiber destruction. Therefore, under no cw-beam nominal-beam-width conditions and for a very limited number of pulsed-beam nominal-beam-width conditions can one expect to reliably operate slow-wire or harp-profile measurements. Furthermore, early in the linac where the beam energy is lower, the amount of beam energy deposited in the fiber is large. Table 3 shows the stopping power and range of protons in carbon. Note that the stopping power of a 6.7 MeV beam is ~32 times that of a 1700 MeV proton beam. The higher stopping power results in greater beam energy deposition into the fiber, higher fiber temperatures, and greater likelihood of fiber damage.

TABLE 3. Proton Beam Stopping Power and Range in Carbon

Beam Energy (MeV)	Stopping Power (MeV cm^2/g)	Stopping Power (MeV/cm)	Range (g/cm^2)	Range (cm)
0.75	> 500	> 1100	<0.002	<0.001
6.7	57.1	126.1	0.068	0.031
20	23.5	51.9	0.48	0.22
100	6.5	14.4	8.6	3.9
211	3.9	8.6	31.8	14.4
469	2.5	5.5	119	54
1700	1.8	4.0	741	336

While not as severe as APT, the SNS linac beam is also too intense for traditional interceptive techniques. For example, Figure 8 shows the SiC-fiber temperature calculated with a 18 mA, 1 GeV SNS beam. The pulsed-beam timing characteristics are a 0.15 ms pulse length and a 60 Hz repetition rate with typical current densities of 0.15 A/cm^2. As in Figure 6, the fiber temperature is well above the nominal 1400 K SiC fiber nominal operating temperature (i.e., shown here to be >1600 K).

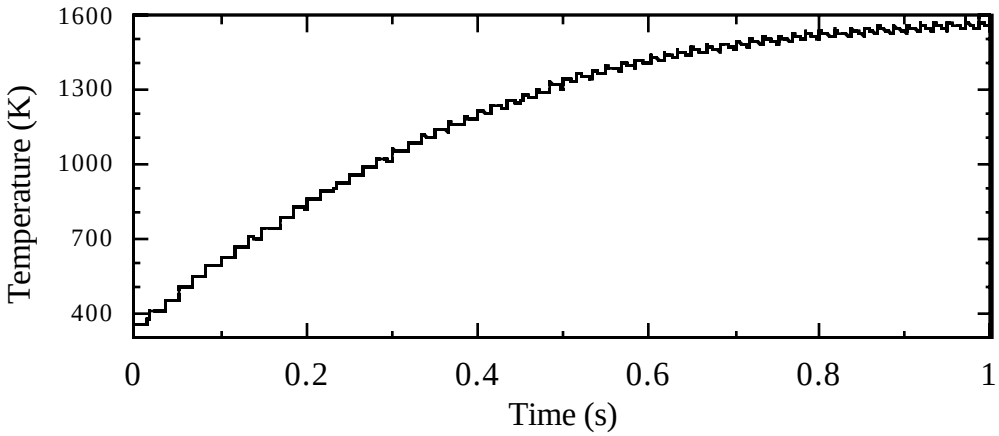

FIGURE 8. This simulation shows how the temperature of a SiC fiber increases to a steady state condition of >1600 K with the SNS beam.

Residual Gas Fluorescence Profile Measurements

At lower beam energies, where deposited beam energies in various materials can be very large, APT and SNS will use a minimally beam-interceptive profile measurement technique. This technique collects and integrates photons resulting from the beam/background-gas interaction. The resultant photon-flux density is dependent on three primary parameters: the beam current density, the beam energy, and the partial background-gas pressure. During the early 1980's several measurements were performed at LANL that characterized these three parameters for proton beams interacting with a nitrogen background gas (9,10). The authors reported that photon radiances of 91 mW/(sr cm^2) at wavelengths near ~400 nm are produced by a 100 mA/cm^2, 80 keV proton beam interacting with partial pressures of nitrogen in the 2×10^{-5} range. Also, this work produced a spectrum of the resultant photons from the beam/gas interaction (shown in Figure 9). The prominent spectral line groups are at ~391 and ~427 nm and are believed to be fast fluorescence process with single-transition excited-state lifetimes of less than 100 ns. These short lifetimes allow for sensing the beam's profile without any apparent beam profile broadening due to non-beam-related phenomenon, such as slower multiple-transition background-gas-ionization processes. During the early 1990's, similar experiences were found at the Ground Test Accelerator (GTA) and Accelerator Test Stand facilities (11). However, it is known that N_2 has metastable states at separate wavelengths which can cause apparent profile broadening. During the operation of GTA, profile broadening was observed as a broad background and thought to be the result of a slow metastable transition.

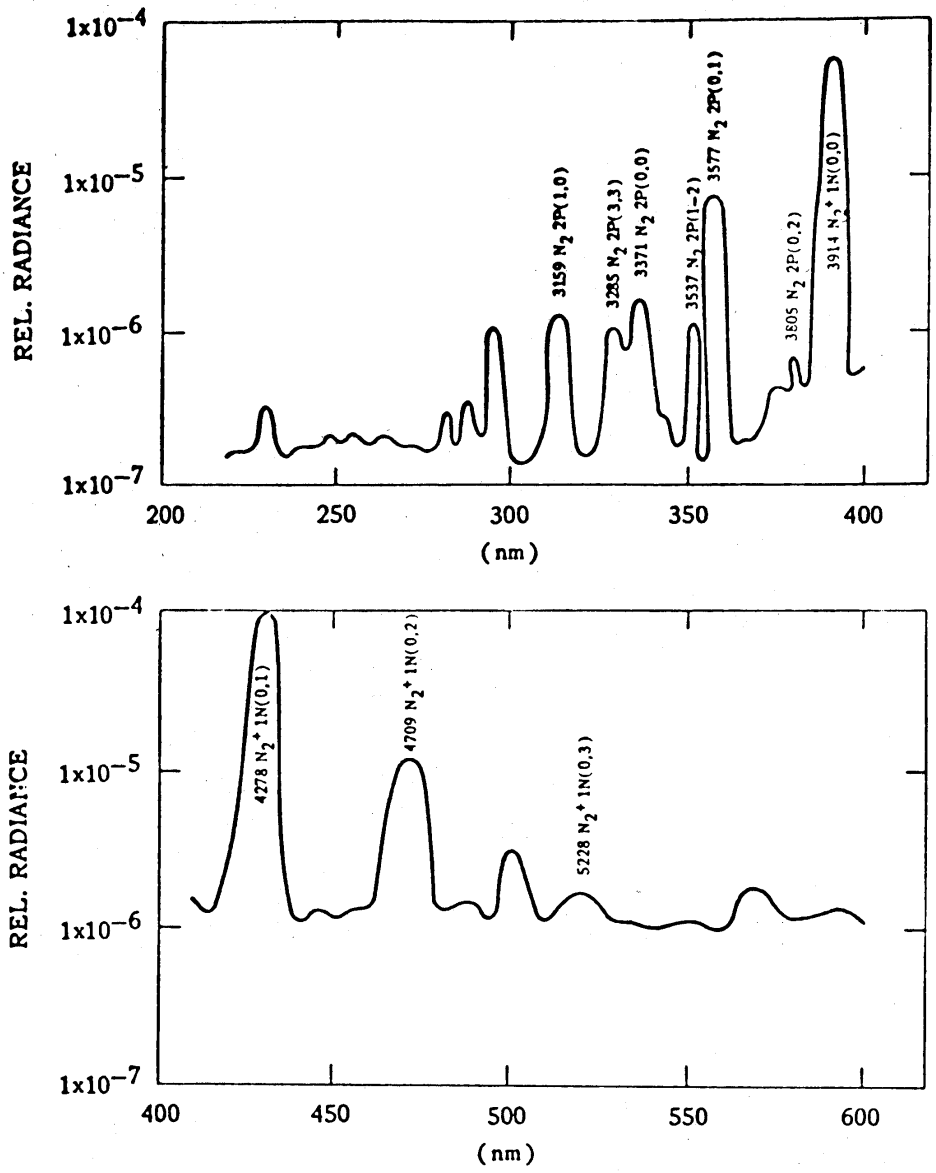

FIGURE 9. The graph is a spectrum of the fluorescence-based photons resulting from a 100 mA/cm^2, 80 keV proton beam interacting with a residual background nitrogen gas.

Table 4 lists calculated values of the viewable radiant power density (assuming a nominal partial pressure of 10^{-6} Torr), the average peak illuminance on a camera faceplate, and the resultant signal-to-noise under cw and 0.1 ms pulsed beam conditions. The cw beam illuminance numbers displayed assume that the NTSC-style cameras are unintensifed and the signal-to-noise numbers are calculated at the distribution peak. The pulsed beam illuminance numbers displayed assume that the NTSC-style cameras are intensified and the signal-to-noise numbers are calculated at the 5% to 10% threshold levels.

TABLE 4. Expected Radiant Power Densities, Average Illuminances, and the Resultant Signal-to-Noise Ratios for 100 mA Beams in 10^{-6} Torr Partial Pressures of Nitrogen

Beam Energy (MeV)	X rms width (mm)	Y rms width (mm)	Radiant Power Density ($\mu W/cm^2$)	Faceplate Illum., cw (lux) [1]	S:N, cw [2]	Faceplate Illum., cw (lux) [3]	S:N, pulsed [4]
6.7	0.9	0.9	1.3	0.2	1000:1	570	16:1
100	1.2	1.2	0.09	0.01	71:1	31	4:1
211	2	1.5	0.019	0.0012	24:1	3.7	1.3:1
469	2.2	1.8	0.0089	0.00051	16:1	1.5	0.8:1
1000	2	1.5	0.00058	0.00038	13:1	1.1	0.7:1
1700	1.2	0.8	0.011	0.0013	25:1	3.5	1.3:1

1. Average faceplate illumination during cw beam operation at the distribution peak.
2. Signal-to-noise ratio during cw beam operation at the distribution peak.
3. Average faceplate illumination during 0.1 ms pulsed-beam operation at the distribution peak.
4. Signal-to-noise ratio during 0.1 ms pulsed-beam operation at the distribution peak.

Flying Wire Profile Measurements

The present baseline profile measurement technique for beam energies greater than ~200 MeV and rms beam widths greater than ~0.5 mm is a flying-wire profile measurement. This somewhat mechanically complicated technique sweeps a wire through the beam with wire velocities greater than a few meters per second. The relative position of the wire is acquired using either an encoder or a tachometer and the beam distribution information is acquired using either prompt ionizing radiation resulting from the wire/beam interaction (e.g., few MeV gammas) or collecting the secondary electrons emitted from the wire. Figure 10 shows the calculated 0.14 mm SiC fiber temperature as a function of time plotted on a logarithmic scale. As the fiber is flown at a 5 m/s velocity through the 100 mA, 1700 MeV, APT beam, the peak fiber temperature of ~1250 K is reached after the wire passes through the 0.7 × 1.5 mm wide beam. The peak temperature can be maintained within a safe operational temperature range as long as neither the wire velocity nor the beam widths is not reduced.

There are several facilities using this technique to acquire proton beam profiles. At Fermi National Laboratory (FNAL), Blokland rotationally translates a 0.033 mm carbon monofilament through their beam while attaining velocities between 2 and 5 meters per second (12). The 540° rotational scans appear to be repeatable to within 1% and the distributed charge is detected sensing prompt gammas with a scintillator material and a photomultiplier tube. CERN also uses several different configurations of the flying-wire technique (13, 14). Bovet reported that the flying-wire scanners used in LEP linearly translates a wire through their beams with speeds of 0.1 to 2 meters per second. CERN personnel have used a variety of wire materials including 0.05 mm Be, 0.036 mm C, 0.01 mm SiC, and 0.007 mm SiO_2. Extensive wire heating studies have been performed and reported in previous workshops and conferences (15). Another type of CERN flying-wire scanner rotationally translates a 0.03 mm carbon fiber through a beam with velocities of 10 to 20 meters per second. The beam charge distribution is detected by either sensing the depleted secondary electrons from the wires or by detecting nuclear

interactions as a result of the beam/wire interaction. Finally, LANL has also partially developed and had limited experience with the flying wire profile measurements (16). In this case, 0.035 mm carbon fibers were rotationally translated through beam regions and peak wire velocities of 5 m/s were attained within the ~300° rotational angular range. The beam charge distributions were detected by sensing the captured secondary electrons. The monitor mechanism was repeatably tested at full speed on the bench to verify the velocity profiles and several crawling or slow-wire tests were performed on a 20 MeV electron beam to investigate background and charge sensing issues. However, no high wire-velocity beam tests were performed.

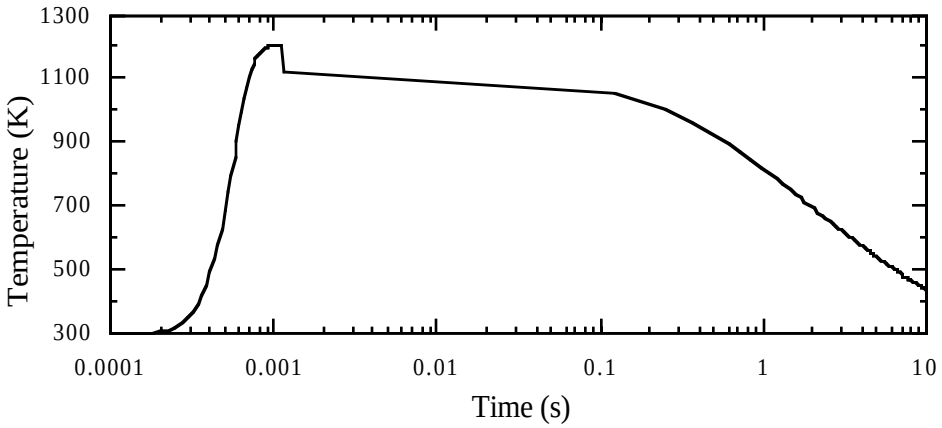

FIGURE 10. This graph plots the calculated temperature of a 0.14 mm SiC fiber or wire as it is flown at a 5 meter-per-second velocity through a 1700 MeV proton beam. The peak fiber temperature of ~1250 K is reached after the wire passes through the 0.7×1.5 mm wide beam.

Residual Gas Ionization Profile Measurements

Residual gas-ionization-profile measurement is another minimally interceptive technique used to measure proton beam profiles. As the beam transports through a evacuated beampipe and the beam's energy is deposited in the background gas, electron-ion pairs are created. An electric field is placed across the beam region so that either electrons or ions are electrostatically accelerated toward a collection device. The electrons or ions are then collected with a series of charge collectors typically in the form of either a multi-wire grid, a phosphor and video camera, or a micro-channel plate (MCP). The collected charge is integrated or averaged over time to reduce the random noise in the detected beam distribution.

The residual-gas-ionization profile-measurement technique has been successfully applied to low-intensity beam-profile measurements. However, for the APT and SNS high current beams, the beam space-charge will cause deep potential wells in the beam region. These potential wells can distort the trajectories of the electrons or ions, and therefore, limit the measurement spatial resolution. An additional magnetic field can focus the ionized electron trajectories and provide a finer profile spatial resolution. One drawback to this particular implementation of the residual gas-ionization-profile measurement is related to the required magnetic field strength. Due the to limited beam line space and the required magnetic field strength, required physically large magnets

may not be placed in the linac, and hence, limit this particular implementation's APT and SNS usage.

One other concern is the quantity of free electron-ion pairs created by the interaction between the beam and background gas. The gas-ionization-cross section is dependent on the background gas partial pressures. If the vacuum is of high quality and background-gas partial pressures are low, the amount of free electron-ion pairs created within a reasonable amount of time can be very small. The lower electron currents require the charge collection detectors integrate the charge distributions over longer time periods to acquire adequate low-noise data. Unfortunately, the charge collection devices have leakage and dark currents that are also integrated with the signal currents. These extraneous noise or background currents limit the maximum integration times, and ultimately, limit the overall operational vacuum range of the profile measurement. One method of overcoming these noise problems as suggested by Jason, of LANL, is to initially discriminate and then count the collected electrons.

There are several facilities using this technique to measure beam profiles. Connolly, of BNL, reported, at the profile measurement workshop, on the gas-ionization profile measurement developed for RHIC (17). This particular implementation uses both a shaped 6.5 kV electric field and 0.2 T magnetic field for confine and accelerate the ionized electrons. The amplitude of the two fields reduces the electrons Larmor radius to <0.3 mm, therefore providing the spatial-resolution lower limit. Witkover, also at BNL, reported on a ionization profile measurement in the AGS that uses a shaped 45 kV electric field to confine and accelerate the collected ions. The collectors have 48 channels per plane with a 1.2 mm pitch. While this implementation is space charge limited for proton operation, it provides useful information for polarized protons and heavy ions.

Bovet at CERN, reported on two different implementations of a ionization profile monitor. K. Wittenburg developed a profile measurement that uses a shaped 22 kV electric field to collect electrons on to a MCP with a phosphor screen and T. Quinteros is developing a measurement that uses both electric and magnetic fields to collect electrons on to a MCP. Forck, of GSI, reported on a profile measurement for their heavy-ion synchrotron that uses a shaped 12.5 kV electric field to accelerate and confine the collected electrons. The collector is a 64 wire grid that uses 0.1 mm diameter wires with a spacing of 1 mm. Hahn, of FNAL, reported on a gas ionization profile monitor in the FNAL booster. This measurement uses a shaped 8 kV electric field that accelerates and confines the collected electrons. The collector used in this measurement is a MCP and typically collects profile information for 1.6 mm rms width beams. They are starting to look at adding a magnetic field in order to further confine or focus the electrons and improve the measurement's spatial resolution.

Other Less Applicable Profile Measurement Techniques

During the profile measurement workshop, Shafer, of LANL, gave a presentation that suggested other possible intense-beam profile measurement techniques and how applicable these other techniques for acquiring intense proton beam profiles.

The other traditional interceptive techniques such as phosphor screens, solid state detector arrays, IR imaging, etc. suffer from the same interceptive-related disadvantages as do slow-wire scanners discussed in the previous sections. All of these techniques are insufficiently robust for long-term usage with these very intense beams.

Various types of non-ionizing radiation-based light cannot be used because the proton beam is not very relativistic (e.g., $\gamma<3$). This means that synchrotron, transition

(e.g., optical transition radiation), and Cherenkov radiation are not suitable for these very intense beams.

One method worth considering is measuring beam width by acquiring second-moment information on the beam from a multi-electrode beam-image-current device, such as a beam-position monitor. This method was first reported by R. Miller of SLAC in the Proceedings of the 1983 Conference on High Energy Accelerators. However, the moment method is very difficult to perform on APT and SNS because of the beam's low emittance and low aspect ratio, and provides only rms-width information (i.e. it provides little or no beam distribution information).

One method that may be of use for SNS is what one might call a laser beam probe (18, 19, 20). This method uses a laser of sufficient power, wavelength, and focused size to photodetach one of the electrons from the H^- ion. The residual neutral-particle beam produced can then be analyzed with a secondary-electron monitor. Various applications of these measurements have been used to measure an H^- beam's longitudinal and transverse phase space. The cross section for H^- beam is very high (i.e., ~40 Mb), however, this is not an applicable solution for APT profile measurements since the there are no electrons in the H^+ particle.

In a similar vein, low-energy ion beams have been suggested as a possible intense beam profile measurement solution and, in fact, CERN personnel are presently investigating this technique.

Electron-beam probes have been developed and reported. Paseru and Ngo performed limited tests with a 1 to 10 keV CRT electron gun and electron currents of 100s of nA (21). They observed deflections for 100 to 350 mA electron beams and showed that the beam positions were measurable. However, no beam size measurements were reported.

There have been several attempts to use various types of vapors and liquid metal beam profile measurements to detect intense beam profiles. CERN personnel reported using a sodium vapor curtain with some limited success (22). Hardek and Gray reported using a magnesium vapor ribbon (23, 24). However, the metal-vapor plates out onto insulating surfaces in vacuum systems, eventually resulting in the shorting out of the ion pumps. There have been reports of SLAC personnel developing a profile measurement that uses a 4 μm diameter pulsed-jet of low-melting point eutectic metal alloy. However, the liquid "wire" broke into beads after 10 or 20 cm, thereby limiting its useful range of operation. These special types of interceptive profile measurements using vapor or liquid metal materials to image the beam generally all suffer from lack of long-term robustness — they require a fair amount of "care and feeding."

CONCLUSIONS

Measuring the transverse beam-profiles of a 100 mA cw, 1 to 3 mm rms width, 1.7 GeV proton beam is a very difficult problem. While there are many profile measurement techniques used for various types of charged particle beams, few of these techniques are applicable to the APT intense-proton-beam profile measurement. There are slightly more applicable measurement techniques for the SNS H^- beam profile measurements (i.e., laser probe technique), however, it too is a very difficult problem. At the present time, there are three possible techniques we are pursuing for detecting the APT and SNS beam profiles. For low beam energies, the residual gas fluorescence technique is expected to provide a sensitive and reliable method of detecting the APT and SNS profiles. However, at higher beam energies the choices become less apparent. The two techniques we are presently pursuing are the flying-wire profile measurement and the residual-gas-ionization profile measurement.

ACKNOWLEDGMENTS

The author would like to thank the attendees and presenters of the Intense Beam Profile Measurement Workshop held in Santa Fe, NM on November 5–6, 1997. Their significant contributions to the workshop topic provided useful and helpful information for the further development of the APT and SNS beam profile measurements.

REFERENCES

[1] Lisowski, P. W., "The Accelerator Production of Tritium Project," presented at the PAC '97.
[2] Lawrence, G. P., and T. P. Wangler, "Integrated Normal Conducting/Superconducting High-Power Proton Linac for the APT Project," presented at the PAC '97.
[3] Schneider J. D., and K. C. D. Chan, "Progress Update on the Lower-Energy Demonstration Accelerator (LEDA)," presented at the PAC '97.
[4] Appleton, B. R., "The National Spallation Neutron Source," presented at the PAC '97.
[5] Simulation run by Robert Ryne, LANSCE-1, LANL.
[6] Simulation run by Edward Gray, LANSCE-1, LANL.
[7] Gilpatrick,J. D., et al., "LEDA and APT Beam Diagnostics Instrumentation,"
[8] Data from Textron Systems Division.
[9] Chamberlin,D. D., et al., "Noninterceptive Transverse Beam Diagnostics," *IEEE Transactions on Nuclear Science*, Vol. **NS-28**, No. 3 (PAC'81), pp. 2347, (June, 1981).
[10] Fraser, J. S., "Developments of Non-Destructive Beam Diagnostics," *IEEE Transactions on Nuclear Science*, Vol. **NS-28**, No. 3 (PAC'81), pp. 2137, (June, 1981).
[11] Sandoval, D., et al., "Fluorescence-Based Video Profile Beam Diagnostics: Theory and Experience," *AIP Conferences Proceedings* **319** (BIW'93), 1993, pp. 273.
[12] Blokland, W., "A New Flying Wire System for the Tevatron," presented at the PAC '97.
[13] Elmfors, P., et al., "Wire Scanners in Large Beam Emittance Accelerators," CERN/PS 97-04, (OP), March 7, 1997.
[14] Boser, J., and C. Bovet, "Wire Scanners for LHC," LHC Project Note 108, October, 1997.
[15] Camas, J., et al., "Observation of Thermal Effects on the LED Wire Scanners," CERN SL/95-20 (BI), May 1995, and *Proc. of the IEEE PAC'95*, Dallas TX (1996).
[16] Wilke, M., et. al., "Status and Test Report on the LANL-Boeing APLE/HPO Flying-Wire Beam-Profile Monitor," Los Alamos LA-12732-SR Status Report, UC-906, Issued: July, 1994.
[17] Connolly, R. C., et al., "A Prototype Ionization Profile Monitor for RHIC," presented at the PAC'97.
[18] R. C. Connolly, et al., "A Transverse Phase-Space Measurement Technique for High-Brightness H^- Beams," NIM, **A312**, pp. 415–419, (1992).
[19] V. W. Yuan, et al., "Measurement of Longitudinal Phase Space in an Accelerated H^- Beam using a Laser-Induced Neutralization Method," NIM, **A329**, pp. 381–392, (1993).

[20] Shafer, R. E., "Laser Diagnostic for High Current H^- Beams," presented at BIW '98, Stanford, California, June, 1998.
[21] Paseru, J. A., and M. T. Ngo, "Nonperturbing Electron Beam Probe to Diagnose Charged Particle Beams," *Rev. Sci. In*., **63**, pp. 3027 (1992).
[22] Vosicki, B., and K. Zankel, "The Sodium Curtain Beam Profile Monitor of the ISR," *IEEE Transactions on Nuclear Science*, **NS-22**, No.3 (PAC'75), pp. 1475 (March, 1975).
[23] Hardek, T., et. al. "Very Low Intensity Storage-Ring Profile Monitor," *IEEE Transactions on Nuclear Science*, **NS-28**, No.3 (PAC'81), pp. 2219 (June, 1981).
[24] Cline, D. B., et. al., "Proton Beam Diagnostics in the Fermilab Electron Cooling Experiment," *IEEE Transactions on Nuclear Science*, **NS-26**, No.3 (PAC'79), pp. 3302 (June, 1979).